ISCI, Volume *19*

Supplemental Information

N-Doped Mo_2C Nanobelts/Graphene Nanosheets Bonded with Hydroxy Nanocellulose as Flexible and Editable Electrode for Hydrogen Evolution Reaction

Guixiang Li, Jiayuan Yu, Ziqian Zhou, Renkun Li, Zhihua Xiang, Qing Cao, Lili Zhao, Xiwen Wang, Xinwen Peng, Hong Liu, and Weijia Zhou

Supplemental Information

Supplemental Figures

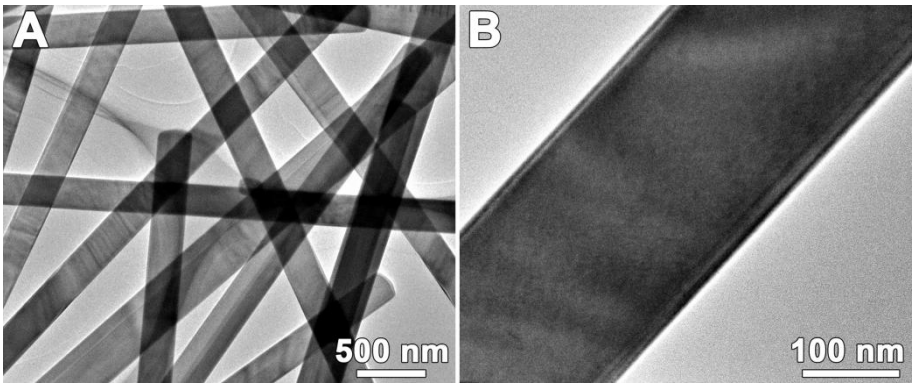

Figure S1. TEM images of MoO_3 nanobelts, related to **Figure 1**.

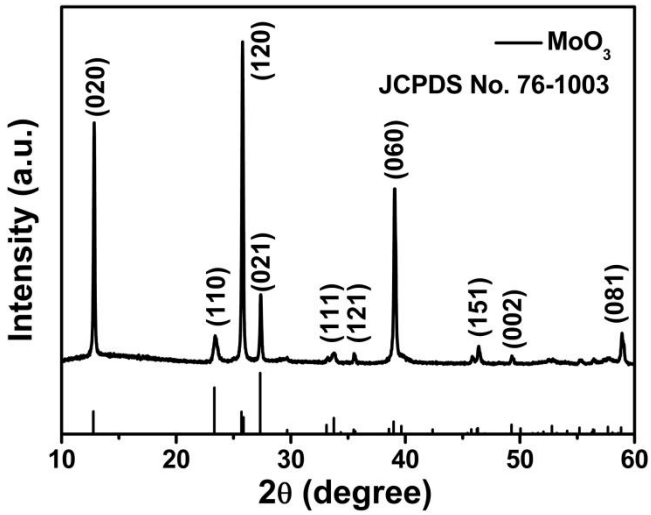

Figure S2. XRD pattern of MoO_3 nanobelt, related to **Figure 1**.

As displayed in **Figure S2**, the typical XRD peaks at around 12.77°, 23.33°, 25.88°, 27.32°, 33.76°, 35.62°, 38.97°, 46.92°, 49.26°, and 58.83° were corresponding to the (020), (110), (120), (021), (111), (121), (060), (151), (002), and (081) planes of MoO_3 (JCPDS No. 76-1003), respectively.

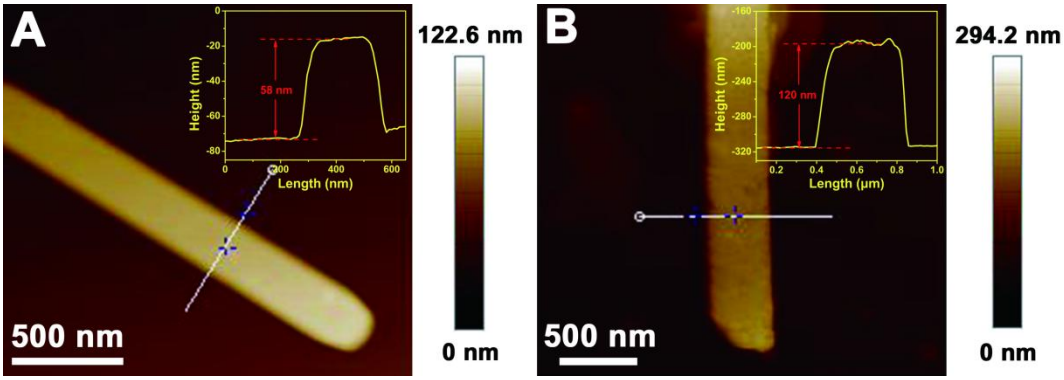

Figure S3. AFM measurement of typical (A) MoO_3 NBs and (B) N-Mo_2C NBs. Inset: Line scans of the height across the corresponding samples, related to **Figure 1**.

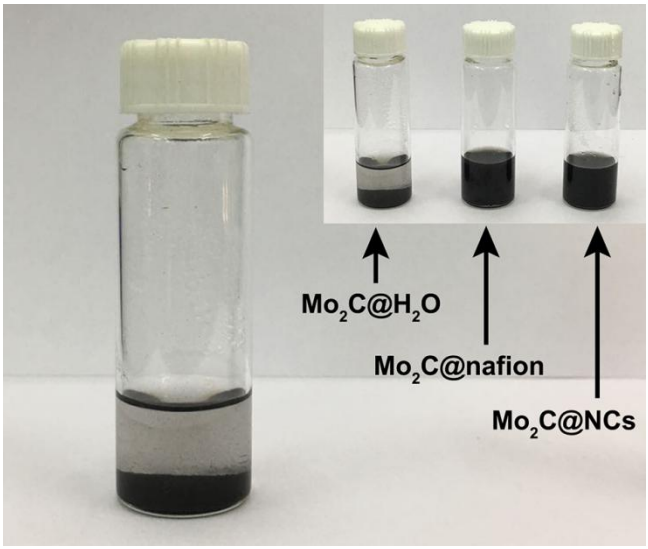

Figure S4. Photo of N-Mo_2C aqueous dispersion after standing for 24 h, related to **Figure 2**.

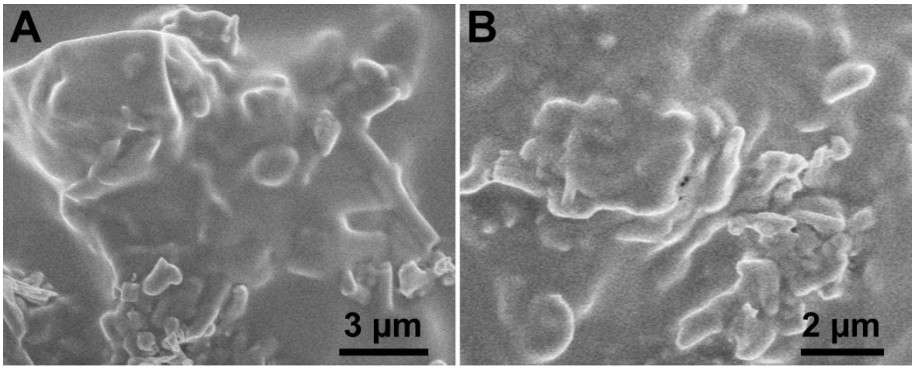

Figure S5. SEM images of N-Mo_2C@nafion aqueous dispersion dried on the GC electrode, related to **Figure 2**.

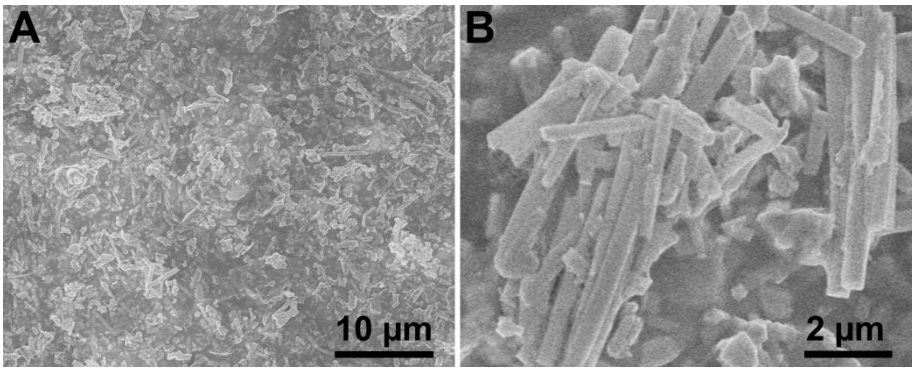

Figure S6. SEM images of N-Mo_2C@NCs aqueous dispersion dried on the GC electrode, related to **Figure 2**.

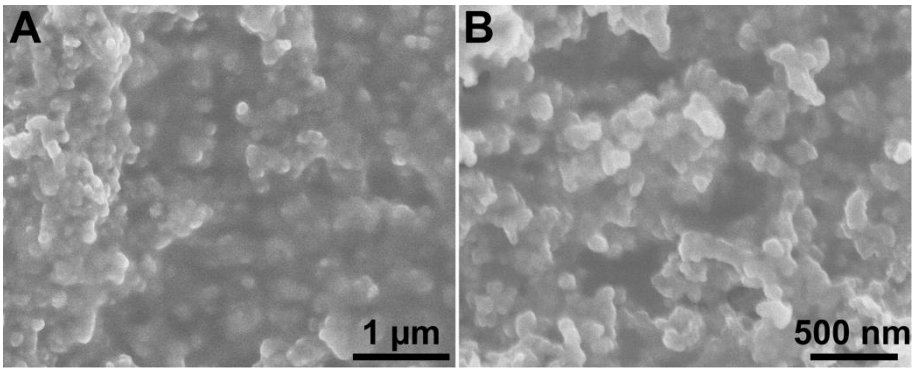

Figure S7. SEM images of 20 wt% Pt/C@nafion aqueous dispersion dried on the GC electrode, related to **Figure 2**.

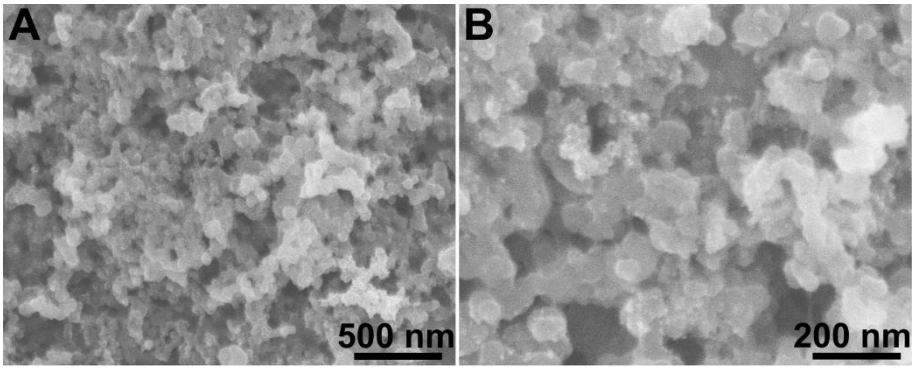

Figure S8. SEM images of 20 wt% Pt/C@NCs aqueous dispersion dried on the GC electrode, related to **Figure 2**.

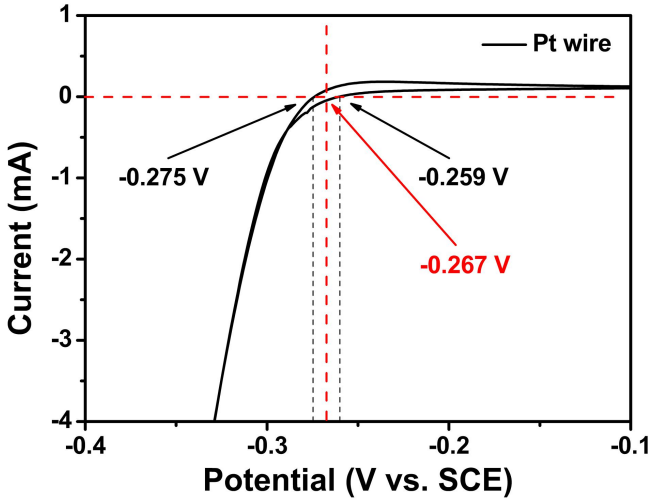

Figure S9. The calibration of reference electrode potential recorded by CV curve, related to **Figure 2**.

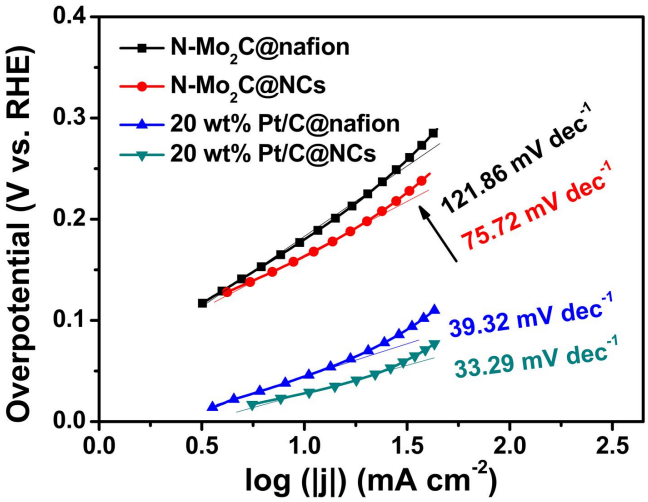

Figure S10. Tafel plots derived from **Figure 2B**, related to **Figure 2**.

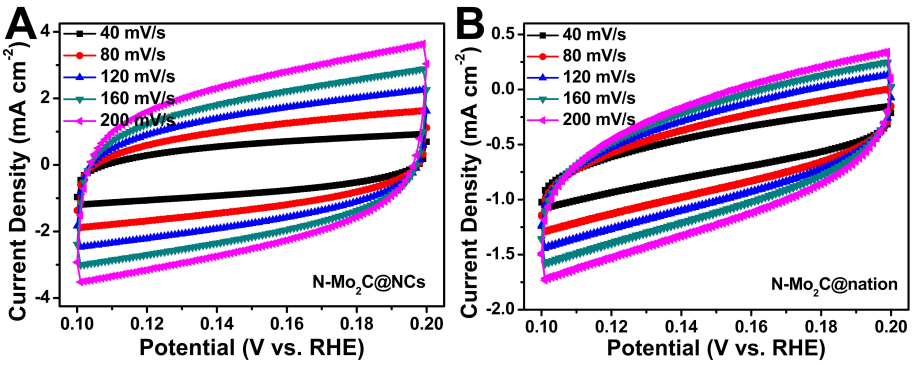

Figure S11. Cyclic voltammograms (CVs) curves of (A) N-Mo_2C@NCs and (B) N-Mo_2C@nafion with different rates from 40 to 200 mV s^{-1} in 0.5 M H_2SO_4 electrolyte, related to **Figure 2**.

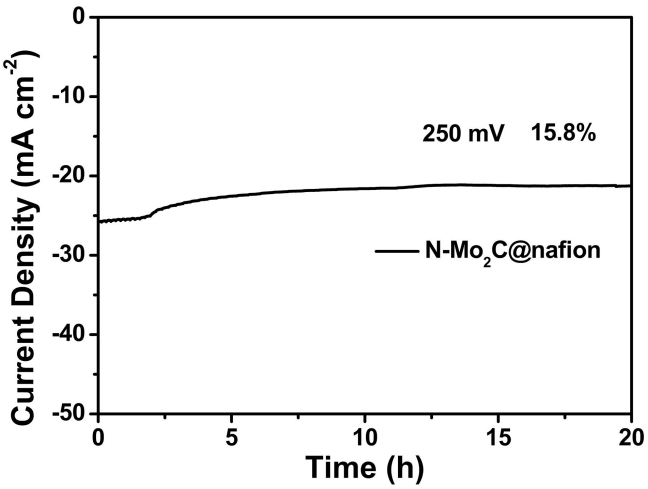

Figure S12. The chronoamperometry curve recorded at the overpotential of 250 mV driven from N-Mo_2C@nafion in 0.5 M H_2SO_4 solution, related to **Figure 2**.

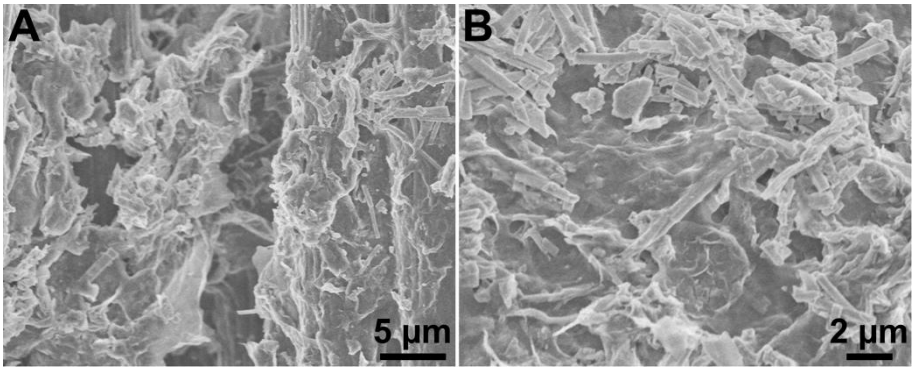

Figure S13. SEM images of N-Mo_2C@NCs loaded on carbon fibers, related to **Figure 2**.

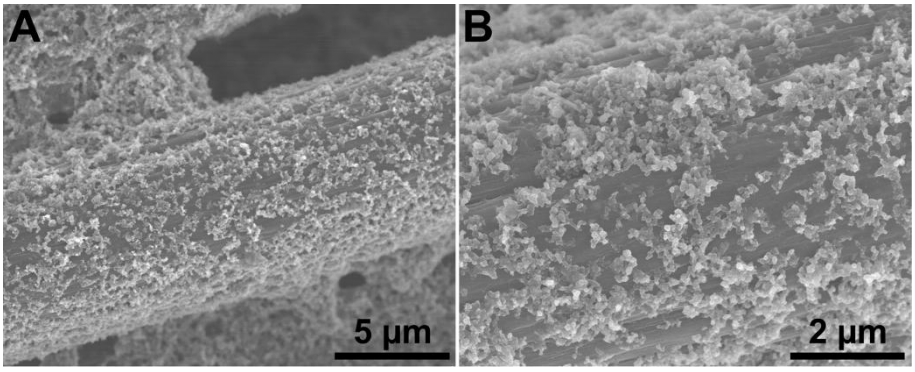

Figure S14. SEM images of 20 wt% Pt/C@NCs loaded on carbon fibers, related to

Figure 2.

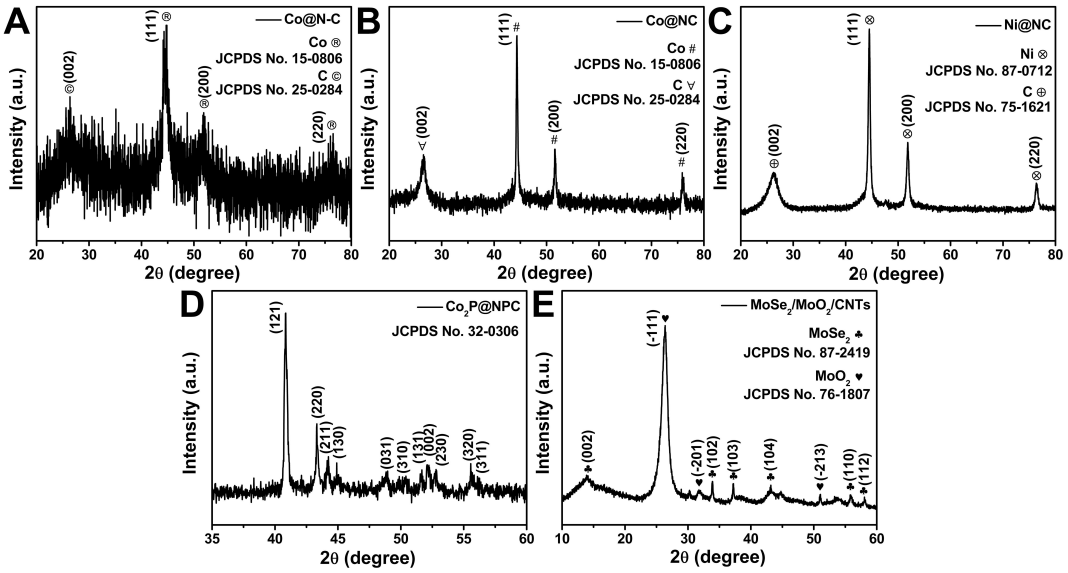

Figure S15. XRD patterns of as-prepared (A) Co@N-C, (B) Co@NC, (C) Ni@NC, (D) Co_2P@NPC, and (E) $MoSe_2/MoO_2$/CNTs catalysts, related to **Figure 2**.

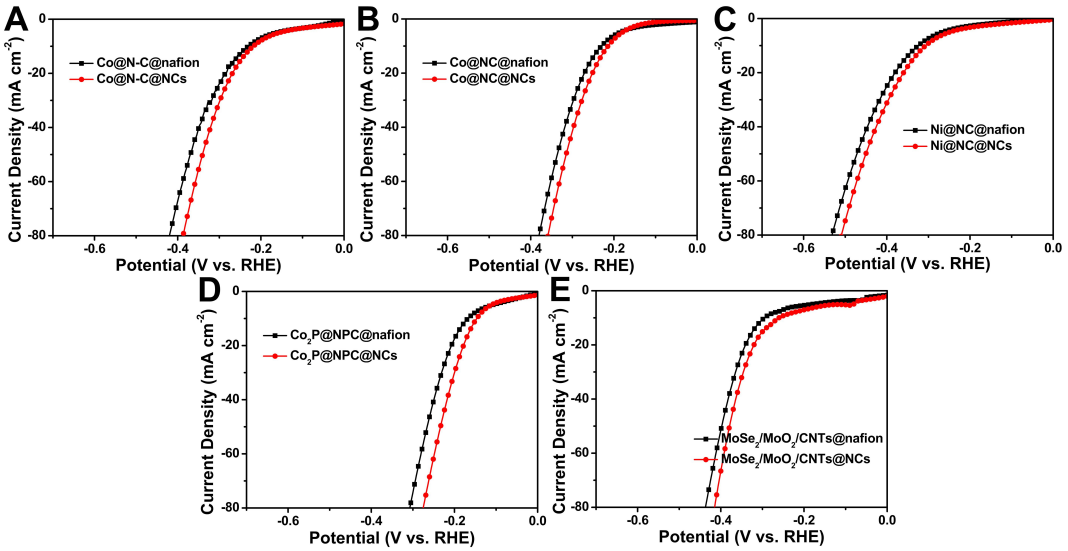

Figure S16. Polarization curves (without *iR* correction) of catalysts bonded with nafion and nanocellulose, respectively, including (A) Co@N-C, (B) Co@NC, (C) Ni@NC, (D) Co_2P@NPC, and (E) $MoSe_2/MoO_2$/CNTs, related to **Figure 2**.

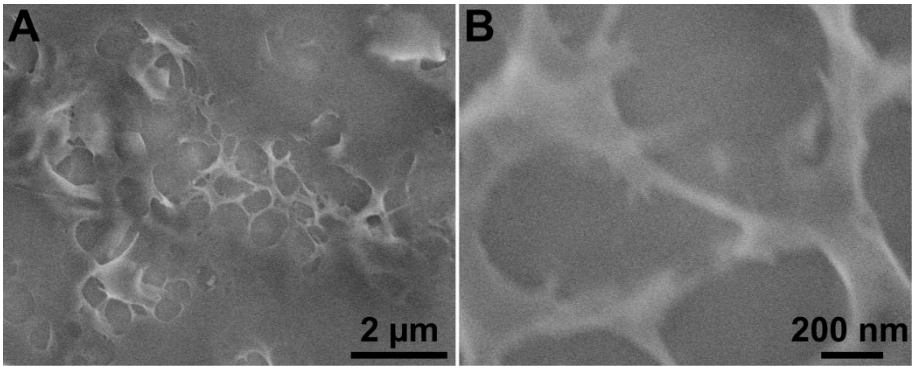

Figure S17. SEM images of pure nanocelluloses, related to **Figure 3**.

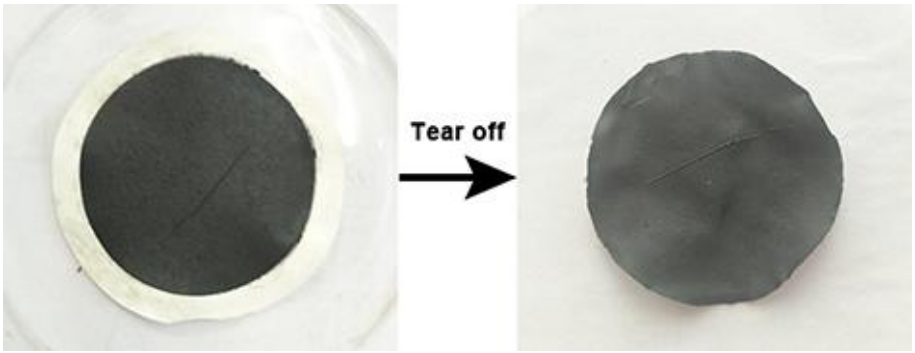

Figure S18. A physical film of N-Mo_2C@NCs was formed by suction filtration only using N-Mo_2C nanobelts and nanocellulose, related to **Figure 3**.

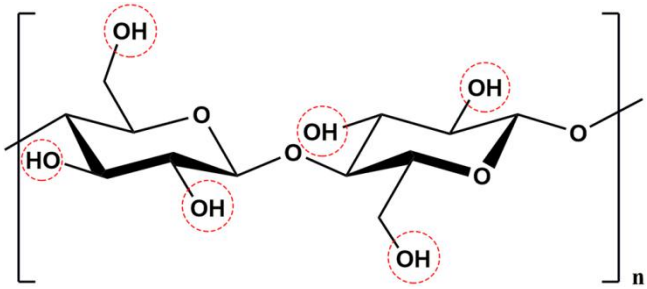

Figure S19. Molecular structure of nanocellulose, related to **Figure 3**.

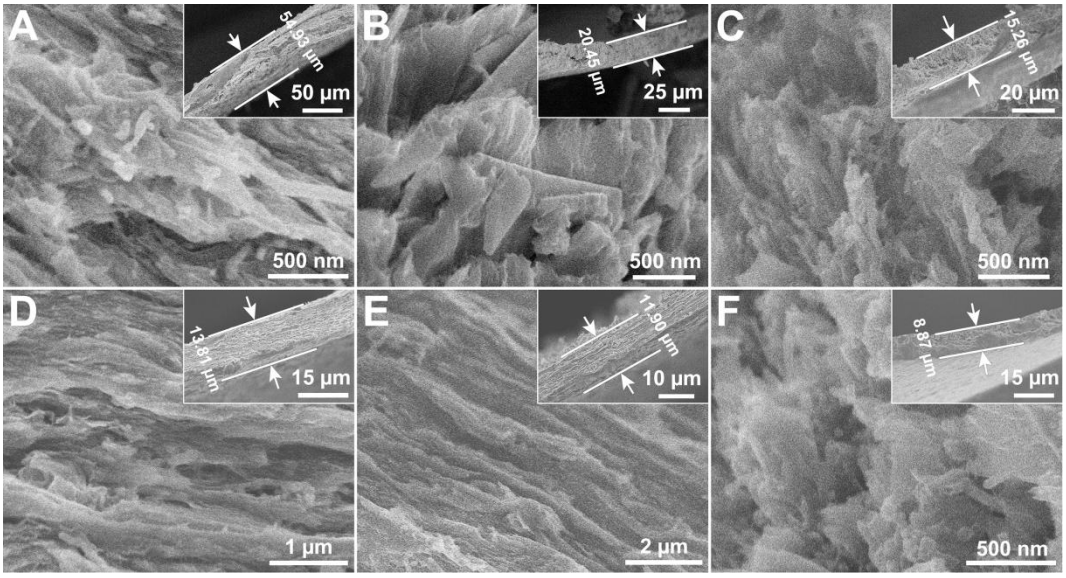

Figure S20. SEM images (A-F) with cross-sectional view of N-Mo_2C/G@NCs films with different thicknesses, related to **Figure 3**.

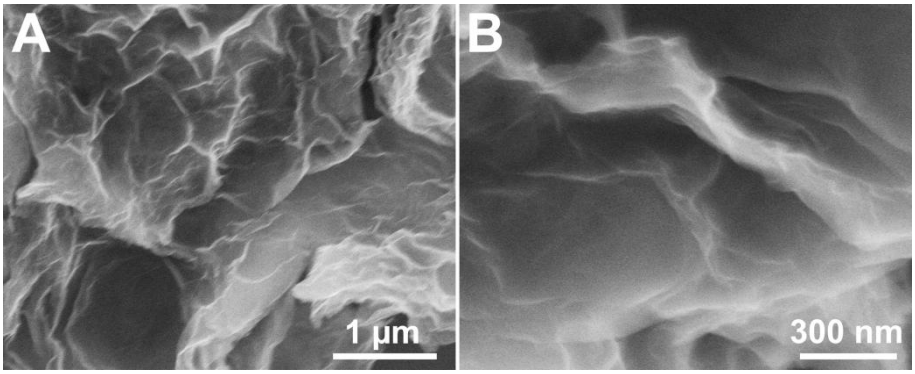

Figure S21. SEM images of graphene nanosheets, related to **Figure 3**.

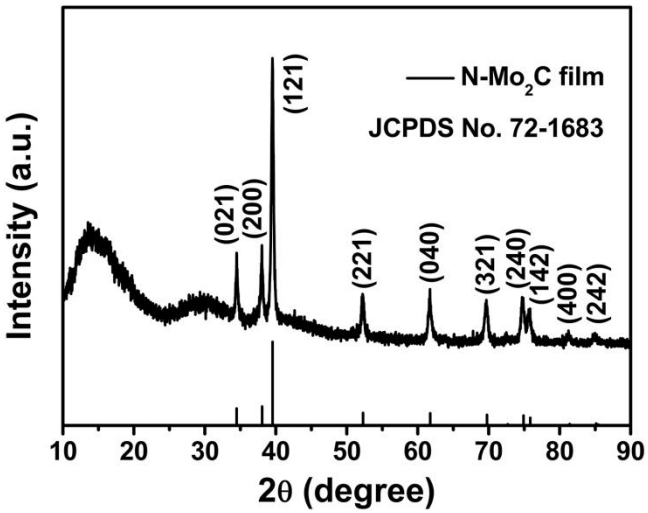

Figure S22. XRD result of N-Mo_2C/G@NCs, related to **Figure 3**.

It could be seen from **Figure S22** that XRD confirmed the prepared flexible films were composed of Mo_2C with characteristic peaks at 34.47° (021), 38.07° (200), 39.53° (121), 52.29° (221), 61.76° (040), 69.77° (321), 74.90° (240), 75.85° (142), 81.42° (400), and 85.12° (242), and the crystalline carbon with characteristic peaks at about 15° and 30°, which was consistent with the crystalline phase of N-Mo_2C powder.

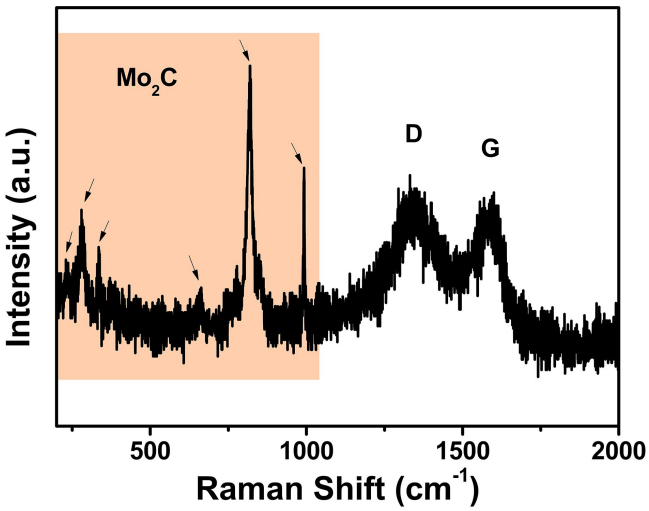

Figure S23. Raman result of N-Mo_2C/G@NCs, related to **Figure 3**.

In **Figure S23**, the N-Mo_2C/G@NCs composite film was further characterized by Raman spectroscopy, which exhibited two distinct peaks located at around 1343 and 1575 cm^{-1}, attributed to the D-band and G-band of the carbon-based matrix,

respectively (Lin et al., 2016). And the film was accompanied by an I_D/I_G value of 1.09, indicating a large amount of disordered carbon existing in the carbon shell drived from N-doped Mo_2C. In addition, it could be observed from **Figure S23** was the presence of Mo_2C, which could further support the successful preparation of N-Mo_2C/G@NCs (Xiao et al., 2014).

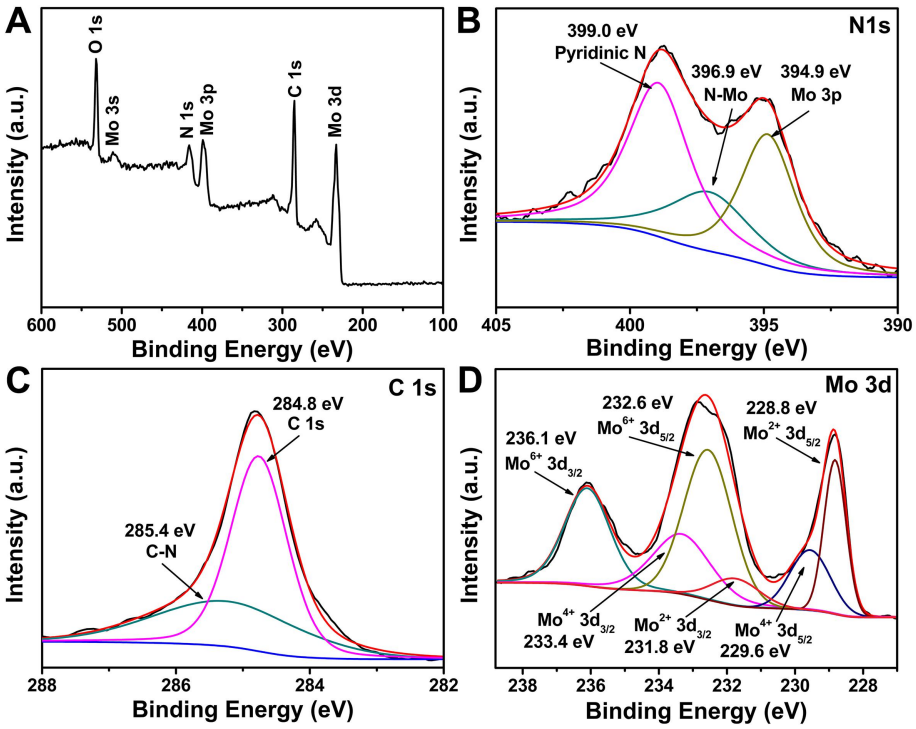

Figure S24. XPS spectra of (A) survey spectrum, (B) N 1s, (C) C 1s, and (D) Mo 3d for N-Mo_2C/G@NCs, related to **Figure 3**.

We accordingly studied the composition of N-Mo_2C nanobelt with X-ray photoelectron spectroscopy (XPS) analysis. As shown in **Figure S24A**, the survey spectra confirmed the presence of C, N, and Mo elements in N-Mo_2C sample. The C 1s, N 1s, and Mo 3d XPS spectra of N-Mo_2C were deconvoluted to estimate the relative contributions of C, N, and Mo species. As illustrated in **Figure S24B**, the N 1s XPS spectrum peak located at 399.0 eV was attributed to pyridinic-N, whereas the peak at 396.9 eV was associated with the N-Mo bonding state (Huang et al., 2018;

Huang et al., 2016). Especially, pyridinic-N exhibited the highest peak in this work and it has been proven to be beneficial for enhancing the electrocatalytic performance of water splitting (Lai et al., 2012). The C 1s peak could be deconvoluted into two peaks centered at 284.8 and 285.4 eV, arising from C-C and C-N, respectively (**Figure S24C**) (Li et al., 2018). Peak deconvolution of Mo 3d verified the existence of Mo_2C (Mo^{2+} $3d_{5/2}$ at 228.8 eV and Mo^{2+} $3d_{3/2}$ at 231.8 eV), MoO_2 (Mo^{4+} $3d_{5/2}$ at 229.6 eV and Mo^{4+} $3d_{3/2}$ at 233.4 eV), and MoO_3 (Mo^{6+} $3d_{5/2}$ at 232.6 eV and Mo^{6+} $3d_{3/2}$ at 236.1 eV), as shown in **Figure S24D** (Wan et al., 2014; Wu et al., 2016). The presence of a significant amount of superficial oxides was not surprising, which seemed to be inevitable due to the surface oxidation of N-Mo_2C nanobelt exposed to air (Huang et al., 2016; Jiang et al., 2017).

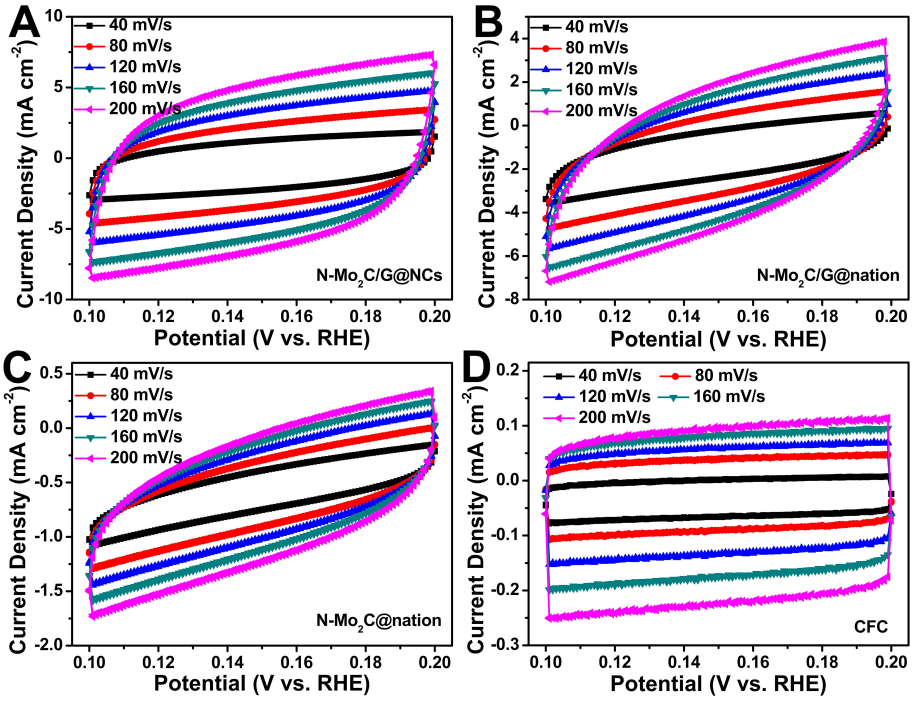

Figure S25. CVs curves of (A) N-Mo_2C/G@NCs, (B) N-Mo_2C/G@nafion, (C) N-Mo_2C@nafion, and (D) bare CFC with different rates from 40 to 200 mV s^{-1} in 0.5 M H_2SO_4 electrolyte, related to **Figure 4**.

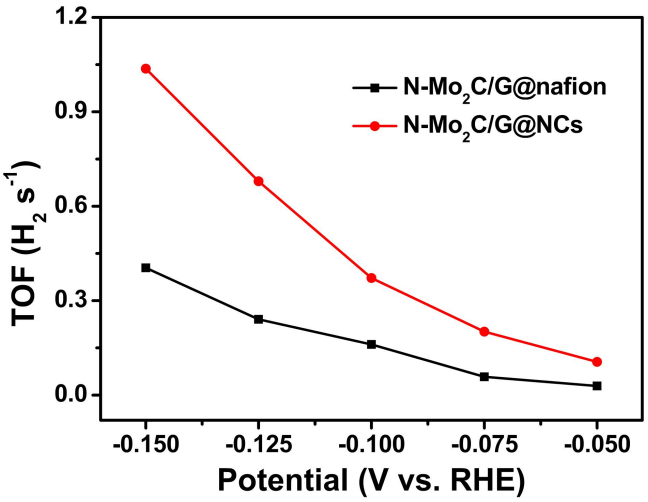

Figure S26. The TOF values plotted against the potential of N-Mo_2C/G@NCs and N-Mo_2C/G@nafion, related to **Figure 4**.

Assuming that all of active sites were entirely accessible to the electrolyte, the TOF values were calculated and plotted against the potential.

The following formula was used to calculate TOF:

$$\mathrm{TOF} = \frac{I}{2Fn}$$

where F and n are the Faraday constant and the number of active sites, respectively; I is the current density of LSV curves.

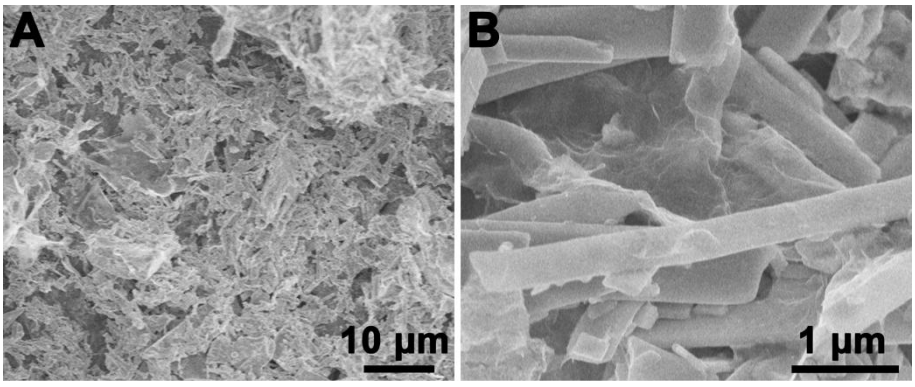

Figure S27. SEM images of N-Mo_2C/G@NCs after i-t testing, related to **Figure 4**.

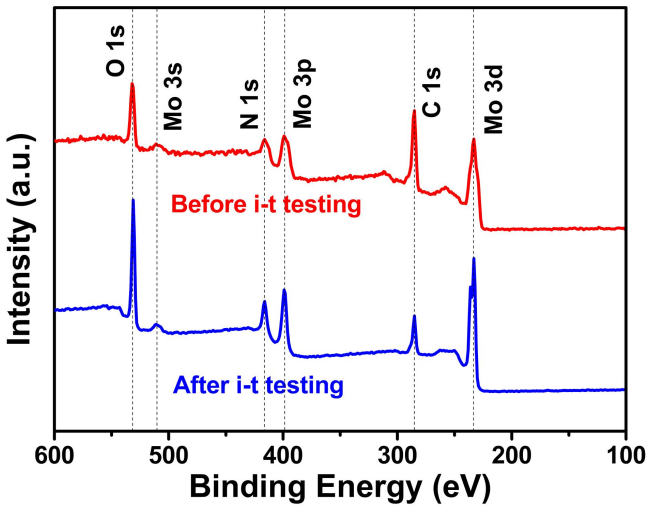

Figure S28. XPS survey spectra for N-Mo_2C/G@NCs before and after the i-t testing, related to **Figure 4**.

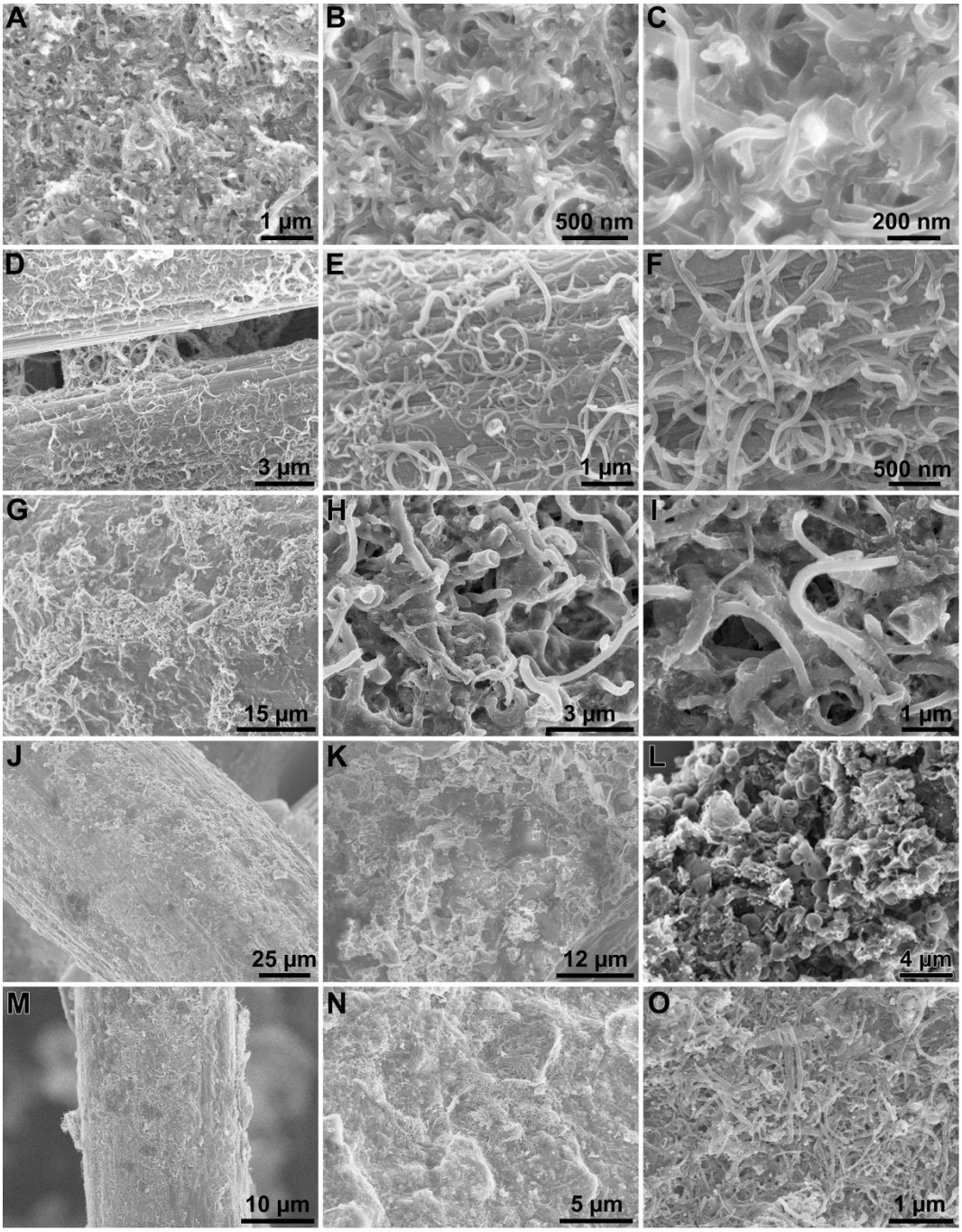

Figure S29. SEM images of (A-C) Co@N-C/G@NCs, (D-F) Co@NC/G@NCs, (G-I) Ni@NC/G@NCs, (J-L) Co_2P@NPC/G@NCs, and (M-O) $MoSe_2/MoO_2$/CNTs/G@NCs loaded on carbon fibers, related to **Figure 4**.

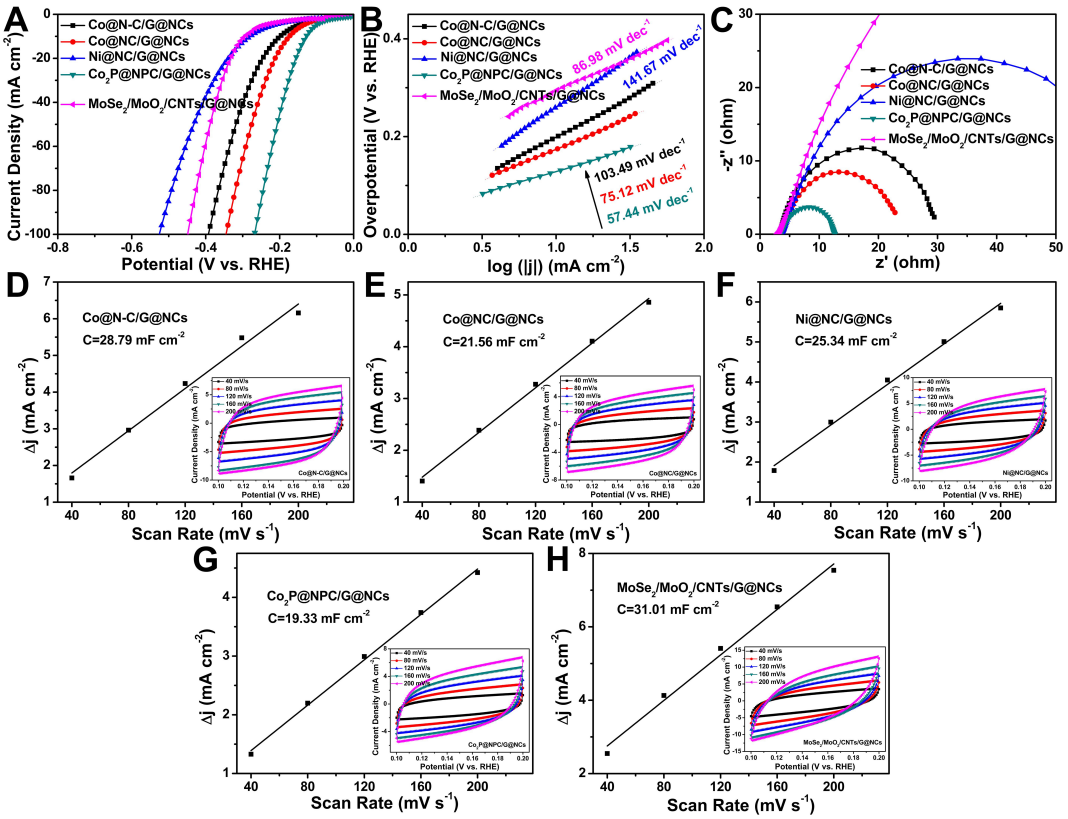

Figure S30. Polarization curves without *iR* correction (A), Tafel plots (B), EIS Nyquist plots (C) of the synthesized Co@N-C/G@NCs, Co@NC/G@NCs, Ni@NC/G@NCs, Co_2P@NPC/G@NCs, and $MoSe_2/MoO_2$/CNTs/G@NCs. The electrical double-layer capacitance and corresponding CVs curves of (D) Co@N-C/G@NCs, (E) Co@NC/G@NCs, (F) Ni@NC/G@NCs, (G) Co_2P@NPC/G@NCs, and (H) $MoSe_2/MoO_2$/CNTs/G@NCs. Related to **Figure 4**.

Transparent Methods

Materials

Mo powder (Mo) and hydrogen peroxide (H_2O_2, 30% w/w) were provided by Aladdin. Dicyandiamide ($C_2H_4N_4$, 99.99%) was obtained from Shanghai Macklin Biochemical Co., Ltd. Graphene (1 mg mL^{-1}) was offered by Nanjing XFNANO Materials Tech Co., Ltd. Nanocellulose dispersion (1%) was purchased from Anhui Sunvo Medicinal Materials Co., Ltd (Hefei, China). And ethanol absolute (EtOH, CH_3CH_2OH) was purchased from Guangdong Guanghua Sci-Tech Co., Ltd., China. Commercial Pt/C (20 wt%) catalyst was kindly supplied by Alfa Aesar. Nafion solution (~5% in a mixture of lower aliphatic alcohols and water) was purchased from Sigma-Aldrich Shanghai Co., and sulfuric acid (H_2SO_4) was obtained from Sinopharm Chemical Reagent Co. The carbon fiber cloth (CFC) was purchased from CeTech Co., Ltd., China. Argon (Ar) was obtained from Guangzhou YIGAS Gases Co., Ltd., China. Deionized (D.I.) water was supplied with a Barnstead Nanopure Water System (18.2 MΩ·cm) and used throughout the experiment.

Synthesis of Molybdenum Oxide Nanobelts (MoO_3 NBs).

In our experiments, molybdenum oxide nanobelts (MoO_3 NBs) as a precursor were prepared following a reported method (Zheng et al., 2009; Yang et al., 2018). In a typical procedure, 1.2 g pure Mo powder was slowly added into a beaker, which contained 10 mL of H_2O_2 aqueous solution (30 wt%). And then it was stirred vigorously for 1 h in an ice-water bath. Soon after, a transparent and yellow solution was formed, containing the water-soluble precursor of $MoO_2(OH)(OOH)$ (Zheng et al., 2009). Furthermore, 62.5 mL of D.I. water was added into the above solution under magnetic stirring for 6 h, and then a homogeneous aqueous solution was

formed. Subsequently, the obtained solution was transferred into a Teflon-lined stainless steel autoclave with a volume of 100 mL, which was hydrothermally treated at 220 °C for 48 h. After the temperature was lowered to room temperature, the mixture was centrifuged to obtain an off-white product of MoO_3 NBs, Finally, the MoO_3 NBs precursor was washed with D.I. water three times, and then dried at 60 °C for 12 h in a vacuum oven.

Synthesis of Nitrogen-doped Molybdenum Carbide Nanobelts (N-Mo_2C NBs).

200 mg of commercial dicyandiamide powders ($C_2H_4N_4$) and 100 mg of obtained MoO_3 NBs were mixed in a ceramic boat and then were sealed, which was placed in a tube furnace with Ar gas to remove air. After that, the mixture was calcined at 450 °C for 2 h and then 800 °C for 2 h to form nitrogen-doped molybdenum carbide nanobelt (N-Mo_2C NBs).

Preparation of the Composite Film of Nitrogen-doped Molybdenum Carbide Nanobelts/Graphene Nanosheets Bonded with Nanocelluloses (N-Mo_2C/G@NCs film).

2 mL of nanocellulose dispersion (1%), 1 mL of graphene (1 mg mL^{-1}) and 1 mL of ethanol absolute were added to a 10 mL glass vials. The weighed 20 mg of synthesized N-Mo_2C NBs powder was transferred to the above glass bottle. The mixture was then placed in an ultrasonic instrument for 30 min to obtain a homogeneously mixed solution. Subsequently, the resulting solution was filtrated dropwise through a filter membrane (pore size of 0.22 μm). Finally, the free-standing flexible and porous N-Mo_2C/G@NCs film could be obtained after drying at room temperature, peeled off from the filter membrane.

In the similar way, the slurry of N-Mo_2C@nafion and N-Mo_2C/G@nafion was obtained. In addition, after undergoing sonication, the mixed solution could be taken

out and dropped onto the carbon fiber cloth, which was dried at room temperature to abtain N-Mo_2C@nafion loaded on carbon nanofiber cloth (N-Mo_2C@nafion/CFC), which was used as electrode because N-Mo_2C@nafion could not form a film by itself. In the similar manner, N-Mo_2C/G@nafion/CFC was also obtained.

Preparation and Film Formation of Other Powder Catalysts

According to the reported literatures, five other powder catalysts were synthesized. Cobalt nanoparticles encapsulated in nitrogen-doped carbon nanotubes (Co@N-C) was obtained by a simple pyrolysis of Co-MOF (ZIF-67) (Yu et al., 2018). Nitrogen-doped carbon nanotube-coated cobalt nanoparticles (Co@NC) and nitrogen-doped carbon nanotube-coated nickel nanoparticles (Ni@NC) were prepared by pyrolysis of cobalt salt and nickel salt with dicyandiamide, respectively (Zou et al., 2014; Zhou et al., 2016). The Co_2P nanoparticles embedded into N, P co-doped carbon shells (Co_2P@NPC) was synthesized by high temperature *in situ* phosphating of Co^{2+}/*saccharomycetes* derived from cobalt ions adsorbed *saccharomycete* cells (Li et al., 2018). $MoSe_2$ nanosheet/MoO_2 nanobelt/carbon nanotube ($MoSe_2$/MoO_2/CNTs) was composed of highly conductive CNTs and hierarchical $MoSe_2$ nanosheets ($MoSe_2$ NSs) on MoO_2 nanobelts (MoO_2 NBs), respectively (Yang et al., 2018). In this part, MoO_2 NBs was obtained from the thermal reduction of MoO_3 NBs and $MoSe_2$ NSs was obtained from the thermal selenization of MoO_2 NBs.

Similarly, as-prepared Co@N-C, Co@NC, Ni@NC, Co_2P@NPC, and $MoSe_2$/MoO_2/CNTs, in the form of powders, were also used to prepare Co@N-C/G@NCs, Co@NC/G@NCs, Ni@NC/G@NCs, Co_2P@NPC/G@NCs, and $MoSe_2$/MoO_2/CNTs/G@NCs films supported on CFC using the similar procedure to the above.

Characterizations

Phase compositions of the as-made materials were measured by D8 Advance (Germany Bruker) X-ray diffraction (XRD) patterns using Cu Kα radiation (λ = 0.15406 nm) at a scanning rate of 0.02°/s in the range of 10° < 2θ < 90°. Raman spectra were got by a LabRAM HR800 spectrometer (Horiba Jobin Yvon, FR.) equipped with a Diode Pump Solid State Laser (wavelength =532 nm). Morphologies of the materials were identified by a field emission scanning electron microscopy (FESEM, MERLIN Compact, Carl Zeiss) and a transmission electron microscopy (TEM, a JEM-2100F Field Emission Electron Microscope, JPN) at an acceleration voltage of 200 kV. X-ray photoelectron spectroscopy (XPS) measurement was carried out on a PHI X-tool instrument (Ulvac-Phi). Brunauer-Emmet-Teller (BET) specific surface area and pore size distribution were attained on a Quantachrome Autosorb-IQ_2 instrument with nitrogen adsorption at 77 K using the Barrett-Joyner-Halenda (BJH) method. The thicknesses of MoO_3 NBs and N-Mo_2C NBs were analyzed by means of atomic force microscopy (AFM, BRUKER Dimension Icon with ScanAsyst, Santa Barbara, USA), operated at room temperature and ambient conditions.

Electrochemical Measurements

All the electrochemical measurements were performed with an electrochemical workstation (CHI 760C, CH Instruments Inc.) in 0.5 M H_2SO_4 aqueous solution using a three-electrode configuration. An Ag/AgCl electrode (SCE, saturated KCl) and carbon rod were used as the reference and counter electrode, respectively. The amount of nafion and nanocellulose were 50 μL nafion/5 mg N-Mo_2C and 500 μL nanocellulose dispersion (1%)/5 mg N-Mo_2C, respectively, when comparing their properties. In order to compare the properties of nafion bonded and nanocellulose

bonded catalysts, and to highlight the advantages of film forming components, while avoiding the effects of non-filming comparative samples during the test (no added nanocellulose), such as N- Mo_2C@nafion and N-Mo_2C/G@nafion, electrochemical tests of non-filming samples were carried out by loading the slurry onto carbon fiber cloth as working electrodes. Polarization curves were achieved by sweeping the potential from 0 to −0.5 V vs. RHE at a potential sweep rate of 5 mV s^{-1}. AC impedance was detected with a frequency range and an amplitude of 10 mV from 0.01 Hz to 100 kHz. The main arc in electrochemical impedance spectroscopy (EIS) spectra was matched utilising a simplified Randles equivalent circuit, which was comprised of a resistance (R_s) in series with a parallel arrangement of a charge-transfer resistance (R_{ct}) and a constant phase element (CPE), and the fitting parameters were appraised through the Levenberg-Marquardt minimization procedure. The electrochemical double layer capacitance was probed by Cyclic voltammetry (CV) at nonfaradaic potentials as another way to reckon the efficient electrochemical active area of HER. Current-time responses were monitored by chronoamperometric measurements by three fixed overpotentials of 286 mV for 100 h, 394 mV for 77 h, and 492 mV for 60 h, respectively. In all electrochemical measurements, the potential of reference electrode was calibrated with respect to a reversible hydrogen electrode (RHE), which was performed in a high-purity H_2 (99.999%) saturated electrolyte with a Pt wire as the working electrode and counter electrode. And then cyclic voltammograms (CVs) were collected at a scan rate of 2 mV s^{-1}, and the average of the two potentials at which the current crossed zero was taken as the thermodynamic potential for the hydrogen electrode reactions. Then in 0.5 M H_2SO_4, it was available that E(SCE) = E(RHE) + (–0.267 V), as shown in **Figure S9**.

Supplemental References

Huang, Y., Ge, J., Hu, J., Zhang, J., Hao, J., Wei, Y. (2018). Nitrogen-Doped Porous Molybdenum Carbide and Phosphide Hybrids on a Carbon Matrix as Highly Effective Electrocatalysts for the Hydrogen Evolution Reaction. *Adv. Energy Mater. 8*, 1701601;

Huang, Y., Gong, Q., Song, X., Feng, K., Nie, K., Zhao, F., Wang, Y., Zeng, M., Zhong, J., Li, Y. (2016). Mo_2C Nanoparticles Dispersed on Hierarchical Carbon Microflowers for Efficient Electrocatalytic Hydrogen Evolution. *ACS Nano 10*, 11337-11343.

Jiang, J., Liu, Q., Zeng, C., Ai, L. (2017). Cobalt/molybdenum carbide@ N-doped carbon as a bifunctional electrocatalyst for hydrogen and oxygen evolution reactions. *J. Mater. Chem. A 5*, 16929-16935.

Lai, L., Potts, J. R., Zhan, D., Wang, L., Poh, C. K., Tang, C., Gong, H., Shen, Z., Lin, J., Ruoff, R. S. (2012). Exploration of the active center structure of nitrogen-doped graphene-based catalysts for oxygen reduction reaction. *Energy Environ. Sci. 5*, 7936-7942.

Li, G., Yu, J., Jia, J., Yang, L., Zhao, L., Zhou, W., Liu, H. (2018). Cobalt–Cobalt Phosphide Nanoparticles@Nitrogen-Phosphorus Doped Carbon/Graphene Derived from Cobalt Ions Adsorbed Saccharomycete Yeasts as an Efficient, Stable, and Large-Current-Density Electrode for Hydrogen Evolution Reactions. *Adv. Funct. Mater. 28*, 1801332.

Lin, H., Liu, N., Shi, Z., Guo, Y., Tang, Y., Gao, Q. (2016). Cobalt-Doping in Molybdenum-Carbide Nanowires Toward Efficient Electrocatalytic Hydrogen Evolution. *Adv. Funct. Mater. 26*, 5590-5598.

Wan, C., Regmi, Y. N., Leonard, B. M. (2014). Multiple phases of molybdenum carbide as electrocatalysts for the hydrogen evolution reaction. *Angew. Chem. Int. Ed. 126*, 6525-6528;

Wu, Z.-Y., Hu, B.-C., Wu, P., Liang, H.-W., Yu, Z.-L., Lin, Y., Zheng, Y.-R., Li, Z., Yu, S.-H. (2016). Mo_2C nanoparticles embedded within bacterial cellulose-derived 3D N-doped carbon nanofiber networks for efficient hydrogen evolution. *NPG Asia Mater. 8*, e288.

Xiao, P., Yan, Y., Ge, X., Liu, Z., Wang, J. Y., Wang, X. (2014). Investigation of molybdenum carbide nano-rod as an efficient and durable electrocatalyst for hydrogen evolution in acidic and alkaline media. *Appl. Catal. B: Environ. 154*, 232-237.

Yang, L., Deng, Y., Zhang, X., Liu, H., Zhou, W. (2018). $MoSe_2$ nanosheet/MoO_2 nanobelt/carbon nanotube membrane as flexible and multifunctional electrodes for full water splitting in acidic electrolyte. *Nanoscale 10*, 9268-9275.

Yu, J., Li, G., Liu, H., Wang, A., Yang, L., Zhou, W., Hu, Y., Chu, B. (2018). Simultaneous water recovery and hydrogen production by bifunctional electrocatalyst of nitrogen-doped carbon nanotubes protected cobalt nanoparticles. *Int. J. Hydrogen Energy 43*, 12110-12118.

Zheng, L., Xu, Y., Jin, D., Xie, Y. (2009). Novel Metastable Hexagonal MoO_3 Nanobelts: Synthesis, Photochromic, and Electrochromic Properties. *Chem. Mater. 21*, 5681-5690;

Zhou, W., Lu, J., Zhou, K., Yang, L., Ke, Y., Tang, Z., Chen, S. (2016). $CoSe_2$ nanoparticles embedded defective carbon nanotubes derived from MOFs as

efficient electrocatalyst for hydrogen evolution reaction. *Nano Energy 28*, 143-150.

Zou, X., Huang, X., Goswami, A., Silva, R., Sathe, B. R., Mikmeková, E., Asefa, T. (2014). Cobalt-embedded nitrogen-rich carbon nanotubes efficiently catalyze hydrogen evolution reaction at all pH values. *Angew. Chem. Int. Ed. 53*, 4372-4376;